N-Doped Graphene Nanoplatelets as Superior Metal-Free Counter Electrodes for Organic Dye-Sensitized Solar Cells

Myung Jong Ju,[†,∥] Jae Cheon Kim,[§,∥] Hyun-Jung Choi,[⊥,∥] In Taek Choi,[†] Sang Gyun Kim,[†] Kimin Lim,[‡] Jaejung Ko,[‡] Jae-Joon Lee,[§,*] In-Yup Jeon,[⊥] Jong-Beom Baek,[⊥,*] and Hwan Kyu Kim[†,*]

[†]Global GET-Future Laboratory and Department of Advanced Materials Chemistry and [‡]Department of Advanced Materials Chemistry, Korea University, 2511 Sejong-ro, Sejong 339-700, Korea, [§]Nanotechnology Research Center & Department of Applied Chemistry, Konkuk University, Chungju 380-701, Korea, and [⊥]Interdisciplinary School of Green Energy/Low-Dimensional Carbon Materials Center, Ulsan National Institute of Science and Technology (UNIST), 100 Banyeon, Ulsan 689-798, Korea. [∥]M.J.J., J.C.K., and H.-J.C. contributed equally to this work.

ABSTRACT Highly efficient counter electrodes (CEs) for dye-sensitized solar cells (DSSCs) were developed using thin films of scalable and high-quality, nitrogen-doped graphene nanoplatelets (NGnP), which was synthesized by a simple two-step reaction sequence. The resultant NGnP was deposited on fluorine-doped SnO_2 (FTO)/glass substrates by using electrospray (e-spray) coating, and their electrocatalytic activities were systematically evaluated for $Co(bpy)_3^{3+/2+}$ redox couple in DSSCs with an organic sensitizer. The e-sprayed NGnP thin films exhibited outstanding performances as CEs for DSSCs. The optimized NGnP electrode showed better electrochemical stability under prolonged cycling potential, and its R_{ct} at the interface of the CE/electrolyte decreased down to 1.73 Ω cm^2, a value much lower than that of the Pt electrode (3.15 Ω cm^2). The DSSC with the optimized NGnP—CE had a higher fill factor (FF, 74.2%) and a cell efficiency (9.05%), whereas those of the DSSC using Pt—CE were only 70.6% and 8.43%, respectively. To the best of our knowledge, the extraordinarily better current—voltage characteristics of the DSSC—NGnP outperforming the DSSC—Pt for the $Co(bpy)_3^{3+/2+}$ redox couple (in paticular, FF and short circuit current, J_{sc}) is highlighted for the first time.

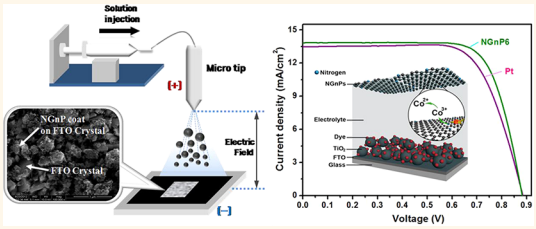

KEYWORDS: N-doped graphene nanoplatelets · charge-transfer resistance · organic dye-sensitized solar cells · electrocatalytic activity · $Co(bpy)_3^{3+/2+}$ redox couple

Dye-sensitized solar cells (DSSCs) are well-known as photovoltaic devices with low-cost, simple fabrication and high power conversion efficiency (PCE).[1−3] However, the components of conventional DSSCs should be replaced with cheaper and eco-friendly materials for practical uses. For instance, organic dyes and carbon-based materials as sensitizers and counter electrodes (CEs), respectively, in DSSCs may bring down manufacturing costs. The CE is one of the most crucial components regulating the PCE by catalyzing the reduction of the redox couples used as mediators to regenerate the sensitizer after electron injection. Platinum (Pt) has been widely employed as the standard CE in DSSCs due to its high catalytic reduction for I_3^-, good chemical stability, and high conductivity. However, the high cost, rarity of Pt and risk of Pt corrosion by the redox species have highlighted the need for low-cost, easily scalable, and more corrosion-stable materials for CEs in DSSCs.

Recently, intensive efforts have been devoted to reduce or replace Pt-based CEs using carbon-based materials such as carbon black,[4] carbon nanoparticles,[5] carbon nanotubes,[6,7] and graphene nanoplatelets[8−12] as metal-free electrocatalysts in DSSCs. The PCE of these materials is still lower than that of the Pt-based CE because of a higher charge transfer resistance (R_{ct}) of the carbon-based CEs toward to the I^-/I_3^- electrolyte and a retardation of the mass transfer of the electrolyte. These persisting problems have been resolved by N-doped graphene sheets[12−16] and reduced graphene oxide.[17−19] Regarding the former case, the introduction of heteroatoms (e.g., nitrogen) into these graphene nanomaterials could further cause electron modulation to provide desirable electronic structures for many electrocatalytic processes of practical significance.[20] N-Doped-carbon

* Address correspondence to jjlee@kku.ac.kr, jbbaek@unist.ac.kr, hkk777@korea.ac.kr.

Received for review February 26, 2013 and accepted May 8, 2013.

Published online May 08, 2013
10.1021/nn4009774

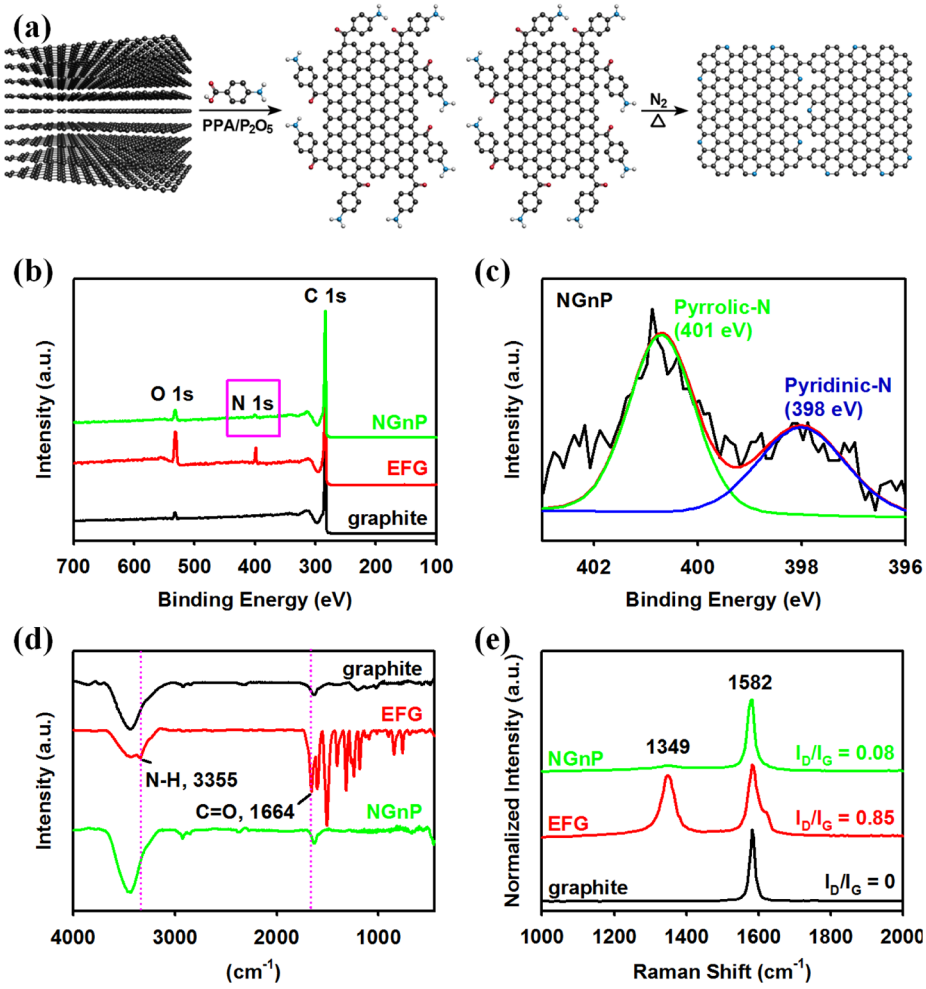

Figure 1. (a) Schematic representation of the synthesis of NGnP *via* edge-selective functionalization of pristine graphite with 4-aminobenzoic acid and subsequent heat treatment under nitrogen atmosphere at 900 °C; (b) X-ray photoelectron survey spectra; (c) high-resolution N 1s spectra; (d) FT-IR (pellet) spectra; (e) Raman spectra.

materials can produce local strains in a hexagonal carbon network, thus leading to structural deformations, and the additional lone pair electrons of nitrogen atoms can bring negative charges with respect to the delocalized π-system of an sp^2-hybridized carbon framework, which can enhance electron-transfer ability and electrocatalytic activities.[21−23] Since defect-free graphene is hardly suitable for the CEs in DSSCs, it is important for the graphene-based CE to balance electrical conductivity for efficient charge transfers and high reduction activity for redox couples, simultaneously. Furthermore, the CE should possess a good chemical stability and low production cost for practicality.[24−26] For highly efficient DSSCs, Ru dyes and I^-/I_3^- redox couple have been substituded by organic sensitizers and Co-complexed redox couples in DSSCs. For instance, the $Co(bpy)_3^{3+/2+}$ redox shuttle in conjunction with an optimized cosensitization of organic dyes as sensitizers demonstrated DSSC with a PCE of 12.3%, which is the current record for this type of device.[27]

Very recently, graphene nanoplatelets (GnP) as the electrocatalyst in Co-bipyridine-mediated DSSCs with Y123-sensitized TiO_2 photoanodes outperformed the Pt−FTO CE particularly in fill factor (FF) and PCE, but they exhibit a lower open-circuit voltage (V_{oc}) than those of the Pt−FTO CE due to the unexpected charge recombination.[19] Here, in order to further improve the electrocatalytic activity of GnP−FTO CEs, in light of the promising heteroatom-containing graphene, nitrogen-doped graphene nanoplatelets (NGnP) were prepared by a simple two-step reaction sequence and they were, for the first time, evaluated as CEs in DSSCs using a $Co(bpy)_3^{3+/2+}$ redox couple. In addition, we used *O*-alkylated-JK-225-organic dye[28] as a sensitizer and a $Co(bpy)_3^{3+/2+}$ redox shuttle exceeding 0.9 V[26,29] of V_{oc} as a redox couple for highly efficient DSSCs. Prior to the actual NGnP uses as CEs in DSSCs, the electrocatalytic activities of the NGnP deposited on fluorine-doped SnO_2 (FTO)/glass substrates for the $Co(bpy)_3^{3+/2+}$ redox couple were systematically examined and discussed with cyclic voltammetry (CV), electrochemical impedance spectroscopy (EIS), linear scan voltammetry (LSV), and chronoamperometry (CA) for the first time. With the optimized NGnP CE, the highest PCE of

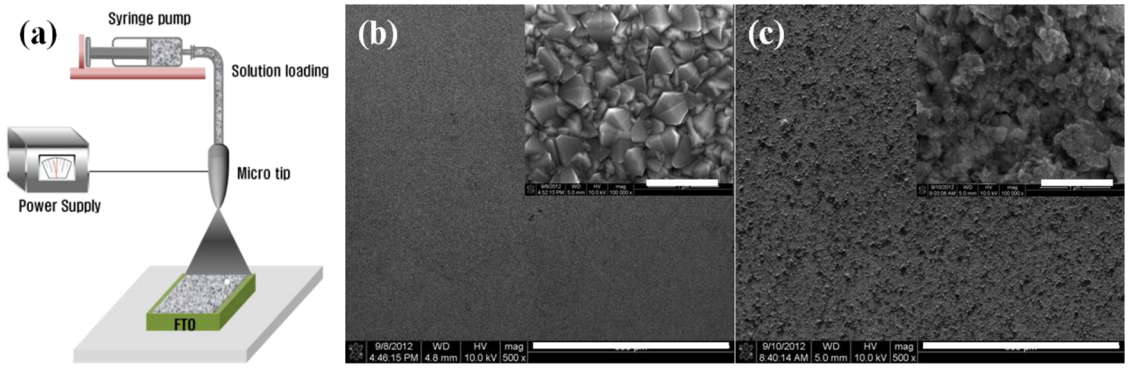

Figure 2. (a) Schematic representation of an e-spray setup. SEM images at low magnification (×1000): (b) bare FTO; (c) NGnP6. Insets are at high magnification (×100000). Scale bars are 300 and 1 μm in the insets.

DSSC was 9.05%, whereas that of DSSC using Pt−CE was 8.43%. More importantly, to our best knowledge, the extraordinarily better current−voltage characteristics (including FF) of the DSSC−NGnP outperforming the DSSC−Pt for the $Co(bpy)_3^{3+/2+}$ redox couple is highlighted for the first time.

RESULTS AND DISCUSSION

Figure 1a is a typical synthetic protocol for the scalable preparation of NGnP by a simple two-step reaction sequence following the synthetic route on the basis of our previous works.[30,31] In brief, edge-selective functionalization of pristine graphite was carried out in poly(phosphoric acid)/phosphorus pentaoxide in the presence of 4-aminobenzoic acid to yield edge-aminobenzoyl functionalized graphite (EFG).[30] The resultant EFG was completely worked up by Soxhlet extractions to minimize unexpected variables. The EFG powder was then heat-treated at 900 °C for 2 h under a nitrogen atmosphere to afford NGnP.[31] During the heat treatment, the 4-aminobenzoyl moieties (4-H_2NPhCO−) that were covalently attached to the edges of the EFG could be *in situ* feedstocks for "C-welding" and "N-doping" to produce NGnP.

The structures of EFG and NGnP were confirmed by X-ray photoelectron spectroscopy (XPS) (Figures 1b and 1c). The nitrogen content of NGnP was found to be 2.79 atomic % (Figure 1b) with a pyrrolic/pyridinic nitrogen ratio of 2/1 (Figure 1c). Unlike graphene oxide (GO) to reduced GO (rGO),[32] FT-IR (Figure 1d) and Raman spectra (Figure 1e) revealed that the graphitic structure of NGnP was almost completely restored as judged by comparison of graphite and NGnP in terms of similar spectra and I_D/I_G ratios. The results imply that edge-selectively functionalized graphene nanoplatelets had minimal damage on their basal plane. Furthermore, scanning electron microscopic (SEM) observations (Figure S1) with energy-dispersive X-ray spectroscopy (EDX, Figure S2) confirmed structural restoration and the presence of nitrogen, respectively.

The NGnP can be readily dispersible in many common organic solvents, and thus it could be deposited on FTO/glass substrates by using an electrostatic spray (e-spray) technique (Figure 2a), which is a simple and practical process for easy control and can deposit thin films on various substrates such as inorganics[33−35] and CNTs.[36] To evaluate the catalytic activities of the NGnP, six different NGnP thin films on FTO were prepared by varying the deposition time. The NGnP-loaded FTO was denoted on the basis of its optical transmittance at 550 nm, T_{550}. As presented in Figure S3, T_{550}'s of NGnP1 NGnP2, NGnP3, NGnP4, NGnP5, and NGnP6 are 83, 69, 61, 44, 31, and 24% in that order (their corresponding deposition time is 1, 2, 3, 5, 7, and 9 min, respectively). Parts b and c of Figure 2c show SEM images of the bare FTO and the NGnP6 film, and the remaining SEM images are presented in Figure S4, showing that more FTO surfaces are covered with the NGnP as deposition time increased.

Figure 3a shows the CV of Pt and NGnP electrodes for the $Co(bpy)_3^{3+/2+}$ redox couple. The electrolyte concentration was 10 times lower than that used in a typical DSSC performance test. In the case of NGnP1−3 electrodes, their electrocatalytic activities were apparently lower than those of the Pt electrode, as judged by peak-to-peak separations (E_{PP}) and current densities. The relatively poor electrocatalytic activities of NGnP1−3 should have originated from their higher R_{ct} at the interface of the electrode and electrolyte solutions due to their small deposition amounts on FTO as observed from SEM images (Figure S4). Interestingly, however, the NGnP4 electrode showed a very similar CV curve shape to that of the Pt electrode in terms of redox peak positions and current densities. Moreover, when the current density and the E_{PP} were compared, the NGnP5 and NGnP6 electrodes exhibited notably higher electrocatalytic performance than that of the Pt electrode. It should be due to an efficient charge transfer by the reduction of R_{ct}, which could be attributable to more NGnP on the FTO surface, suggesting that their intrinsic electrocatalytic activities are expected to be superior to

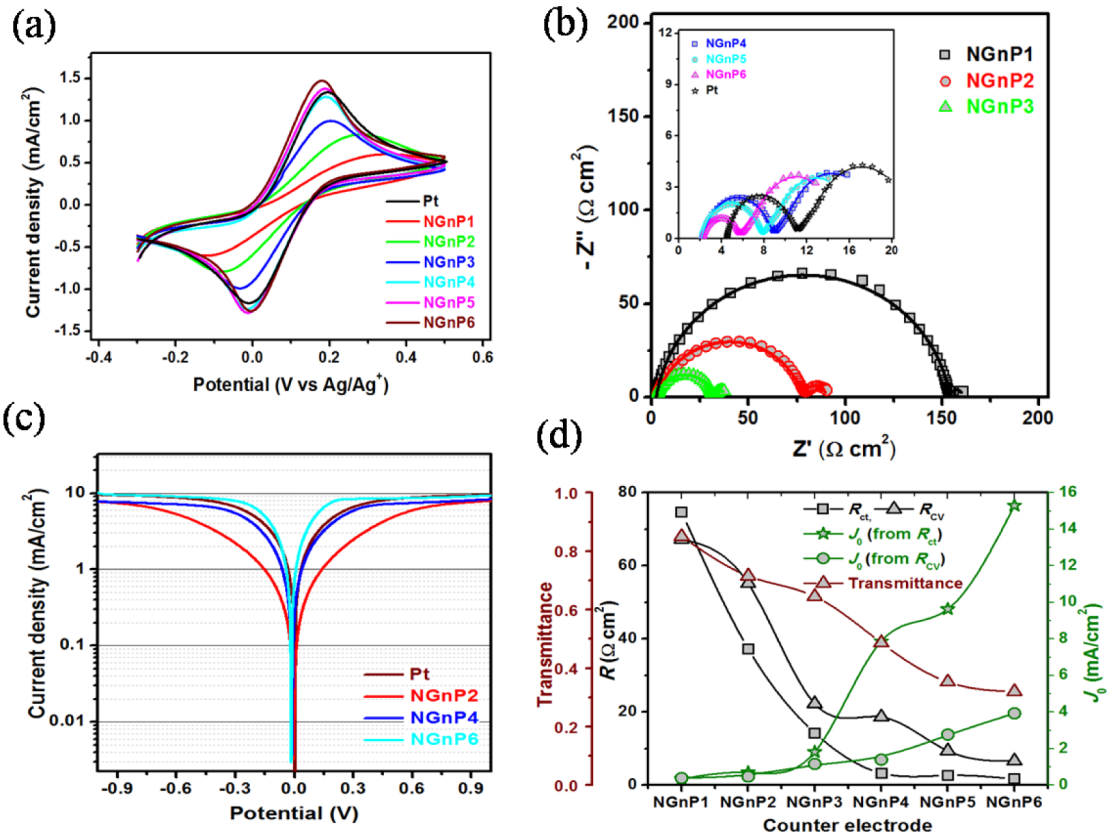

Figure 3. (a) Cyclic voltammograms obtained at a scan rate of 10 mV/s for the oxidation and reduction of the $Co(bpy)_3^{3+/2+}$ redox couple using the Pt and NGnP working electrodes, a Pt wire as the CE, Ag/Ag^+ as the reference electrode, and 0.1 M $LiClO_4$ was used as supporting electrolyte; (b) Nyquist plots of the NGNP1−3 dummy cells measured at 0 V from 10^6 to 0.1 Hz. The inset is the Nyquist plots of the Pt and NGnP4−6 dummy cells; (c) Tafel plots of dummy cells between ±1.0 V with a scan rate of 10 mV at room temperature; (d) charge-transfer resistances (R_{ct}, R_{CV}) and exchange current density (J_0) from EIS and Tafel plots in accordance with the transmittance of NGnP electrodes.

the Pt CEs in actual DSSCs using $Co(bpy)_3^{3+/2+}$ redox couple.

On the basis of promising CV results, the electrocatalytic activity of the CE in DSSCs can be conveniently evaluated by using a symmetrical dummy cell, in which a thin layer of the electrolyte solution is sandwiched between two identical electrodes to be tested as CEs of the DSSCs (Figure S5).[37−39] Figure 3b shows the Nyquist plots obtained by the NGnP dummy cells for the $Co(bpy)_3^{3+/2+}$ redox couple. EIS parameters obtained from the semicircles appeared at the first high-frequency region through an equivalent circuit presented in Figure S6. The results are summarized in Table 1 and Table S1 (Supporting Information). For example, the NGnP6 electrode displayed the EIS parameters, R_s = 1.10 Ω cm², R_{ct} = 1.73 Ω cm², $1/B = 1.88 \times 10^{-4}$ Ss^{β}, and β = 0.76. As expected, the R_{ct}'s of the NGnP electrodes varied in proportion to the amount of NGnP deposition, and the CPE parameter, B was roughly proportional to R_{ct}, which suggested that the electrocatalytic activity was closely related to the amount of NGnP. Moreover, the decrease of CPE parameter β with the amount of NGnP on FTO suggested that the surface roughness decreases with the amount of NGnP deposited on FTO. Therefore, the trade-off condition

TABLE 1. Electrochemical Parameters of Sample Electrodes in Symmetrical Dummy Cells

	LSV		EIS			
CE	R_{CV} (Ω cm²)	J_0 (mA/cm²)	R_s (Ω cm²)	R_{ct} (Ω cm²)	CPE:1/B (Ss^{β})	J_0 CPE:β (mA/cm²)
Pt	9.96	2.58	2.24	3.15	8.76×10^{-5} 0.85	8.16
NGnP2	55.16	0.47	1.24	37.96	3.93×10^{-5} 0.83	0.68
NGnP4	18.65	1.38	1.09	3.32	1.28×10^{-4} 0.79	7.74
NGnP6	6.62	3.88	1.10	1.73	1.88×10^{-4} 0.76	14.90

between the enhancement of catalytic activity and the minimization of the surface roughness at the optimum thickness exists in the present NGnP CE. The R_{ct} is a useful parameter to evaluate the catalytic performance of the CE materials in DSSCs.[40] If the CE has an exchange current density (J_0) of 20 mA/cm², this J_0 value corresponds to an R_{ct} = 1.3 Ω cm² (n = 1) at room temperature. As described in eq 1, the J_0 varies inversely with R_{ct}, where R is the gas constant, T is the absolute temperature, n is the number of electrons, and F is the Faraday constant.

$$J_0 = \frac{RT}{nFR_{ct}} \quad (1)$$

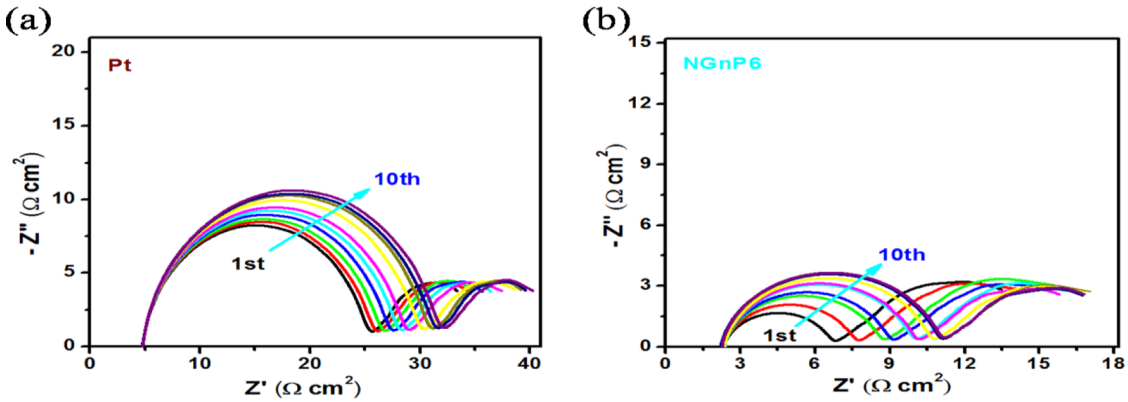

Figure 4. Electrochemical stability of sample electrodes in $Co(bpy)_3^{3+/2+}$ electrolyte solution in acetonitrile under cycling potential: (a) Pt and (b) NGnP6 dummy cells. The sequence of measurements was as follows: 2 × CV scans (from 0 V → 1 V → −1 V → 0 V at a scan rate of 50 mV/s) followed by 30 s relaxation at 0 V and then EIS measurement at 0 V for 10 times.

For the NGnP5 and NGnP6 CEs as well as the Pt CEs, the R_{ct} values were 2.77, 1.73, and 3.15 Ω cm^2, respectively. The corresponding J_0 values, calculated from eq 1, were 9.28, 14.90, and 8.16 mA/cm^2 in that order (Table 1). The electrochemical $Co(bpy)_3^{3+}$ reductions on the NGnP5 and NGnP6 CEs were significantly enhanced compared with that of the Pt CEs. As shown in Figure S7 (Supporting Information), between the J_0 values and the $1/R_{ct}$ or $-\log T_{550}$ of the NGnP electrodes there was a linear relationship.

The R_{ct} at the interface of the CE/electrolyte as well as the diffusion constant of the redox couple in the bulk electrolyte solution are important parameters for the efficiency of a DSSC.[37] The semicircles in the low-frequency region exhibited a similar shape for NGnP and Pt electrodes (Figure 3b). The curve fitting of the second semicircles from the Nyquist plots to Z_W with an EC allows the determination of the $Co(bpy)_3^{3+}$ diffusion coefficients (eq S2, Supporting Information), which were found to be 3.2×10^{-6} and 3.6×10^{-6} cm^2/s for the NGnP6 and Pt, respectively. These similar values between the NGnP and Pt electrodes for mass transfer indicated that ionic diffusion in the bulk electrolyte solution is independent of their catalytic activity. Figure 3c shows the representative Tafel plots recorded on dummy cells, and the rest are presented in Figure S8 (Supporting Information). The slope of the Tafel plots at the potential around 0 V characterizes the overall cell resistance (R_{CV}) that can be attained at low current densities.[41] The R_{CV} and J_0 values calculated from the Tafel plots are also summarized in Table 1.

The curve at intermediate potential with a sharp slope can be attributed to the Tafel zone, where both the anodic and cathodic branches show a larger slope for the NGnP6 than the Pt, indicating a higher J_0 value of the NGnP6. As shown in Figure 3d, a similar trend was observed in R_{ct} and R_{CV} values, which were calculated from both EIS and the Tafel plots of the NGnP dummy cells.

Moreover, the limiting current density (J_{lim}) depends on the diffusion coefficient of redox couples in DSSCs. The Tafel plot of the NGnP6 exhibited a plateau at a J_{lim} of *ca.* 9.4 mA/cm^2, whose value was attributed to mass transport in the electrolyte solution as expressed in eq 2

$$J_{lim} = \frac{2nFcD}{\delta} \quad (2)$$

where n is the number of electrons in the $Co^{3+/2+}$ redox couple, F is the Faraday constant, c is the $Co(bpy)_3^{3+}$ concentration, D is the diffusion coefficient, and δ is the distance between electrodes in a dummy cell. The calculated diffusion coefficient for the NGnP6 electrode (c = 50 mmol/L and δ = 60 μm) was *ca.* 5.9×10^{-6} cm^2/s, whose value is in accordance with the values calculated from the EIS measurement and CA plot shown in Figure S9 (Supporting Information).

For evaluation of electrochemical stability, freshly assembled dummy cells were first measured with EIS at room temperature, and then the dummy cells were subjected to CV cycles followed by EIS measurements. Figure 4 shows the electrochemical stability of both NGnP6 and Pt under cycling potential in $Co(bpy)_3^{3+/2+}$ solution in acetonitrile. There were no noticeable changes in both R_s in the high-frequency region and the semicircles in the low frequency region, suggesting that the cycling potential had no influence on R_s and the mass transport in the electrolyte solution. The R_{ct} for the freshly assembled Pt was initially 3.15 and 10.15 Ω cm^2 in the first cycle, but it was gradually increased up to 13.38 Ω cm^2 in the final cycle. On the other hand, the freshly assembled NGnP6 exhibited an R_{ct} of 1.73 and 2.15 Ω cm^2 in the first cycle, and slightly increased up to 4.35 Ω cm^2 in the final cycle. Thus, the NGnP6 had better electrochemical stability than that of the Pt electrode in $Co(bpy)_3^{3+/2+}$ medium.

On the basis of in-depth evaluation of the NGnP electrodes, the photocatalytic activities of the NGnP electrodes as the CEs in the actual devices were

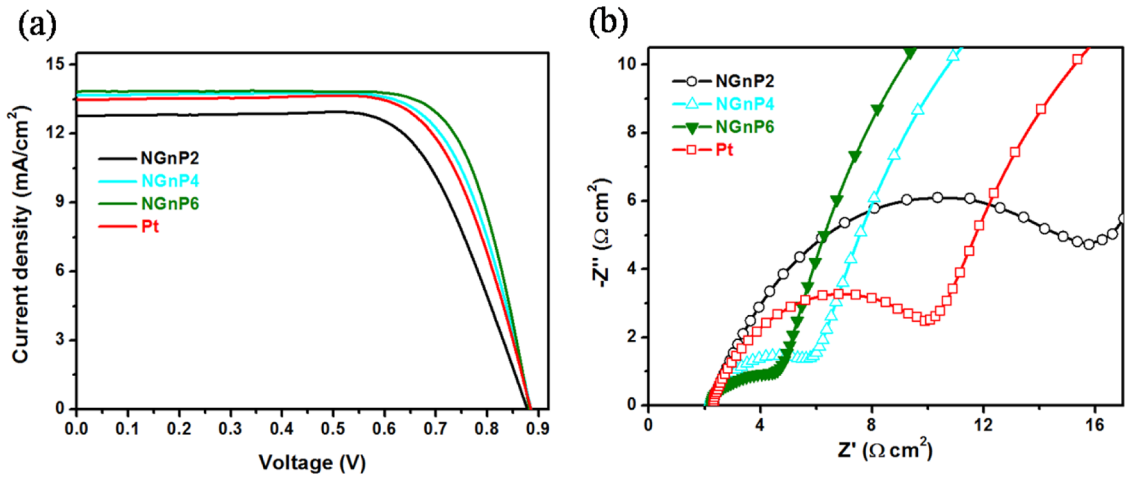

Figure 5. (a) Current−voltage characteristics of the DSSCs with Pt and NGnP CEs under one sun illumination (AM 1.5G). The TiO_2 film thickness and active area are 9(6 + 3) μm and 0.16 cm^2 with a black metal mask, respectively. (b) Nyquist plots of the DSSCs obtained at a forward bias of −0.80 V under dark conditions.

TABLE 2. Photovoltaic Performance of the DSSCs with Pt and NGnP CEs under 1 sun Illumination (AM 1.5)

CE	J_{sc} (mA/cm^2)	V_{oc} (mV)	FF (%)	PCE (%)
Pt	13.48	885	70.6	8.43
NGnP2	12.78	878	68.1	7.63
NGnP4	13.67	885	71.3	8.63
NGnP6	13.83	883	74.2	9.05

performed in $Co(bpy)_3$-mediated solar cells with *O*-alkylated-JK-225-sensitizer[28] and a multifunctional coadsorbent HC-A[42−44] as a coadsorbent instead of deoxycholic acid (DCA), which is commonly used in DSSCs (see Figure S10 and Table S2, Supporting Information). Figure 5a shows the representative current−voltage characteristics with the numerical data summarized in Table 2, and the rest of the data are presented in Figure S10a and Table S2 (Supporting Information). The Pt-based reference DSSC exhibited a short circuit current (J_{sc}) of 13.48 mA/cm^2, an open crcuit voltage (V_{oc}) of 885 mV, a fill factor (FF) of 70.62%, and a PCE of 8.43%. The DSSC with the NGnP6 CE showed an much higher J_{sc} of 13.83 mA/cm^2 and a FF of 74.19%, and a PCE of 9.05%, except a slightly lower V_{oc} of 883 mV. This indicates that the DSSC with the NGnP6 CE enhanced the current−voltage characteristics of organic DSSCs, in particular, FF and J_{sc}, except for the similar V_{oc}. As shown in Figure 5a and Table 2, the DSSC with NGnP2 CE exhibited a slightly lower performance, while the DSSCs with NGnP4,6 CEs outperformed the DSSC with the Pt CE, which might also be due to the decrease in R_{ct} at the interface of the CE/electrolyte solution. Thus, it is now obvious that the NGnP4 and 6 CEs have a higher electrocatalytic activity stemming from lower R_{ct} than that of Pt CEs. These data clearly indicate the important role of nitrogen doping for carbon-based metal-free CEs in DSSCs.

To better understand the improved performance of NGnP CEs for DSSCs, EIS measurements were carried out using the same devices. Figure 5b shows the representative Nyquist plots obtained at the high frequency region, and the remaining plots are presented in Figure S10 (Supporting Information) and numerical data summarized in Table S3 (Supporting Information). The semicircles of NGnP4 and 6 are discriminately smaller than those of the Pt CE, wheares NGnP2 has a much larger semicircle. From the first semicircle, the R_s and R_{ct} for the NGnP2 CE are 2.32 and 14.97 Ω cm^2, respectively. On the other hand, R_s (2.09, 2.11 Ω cm^2) and R_{ct} (4.26, 3.06 Ω cm^2) for the NGnP4,6 are lower than the corresponding values for the Pt CE (R_s = 2.27 Ω cm^2, R_{ct} = 8.44 Ω cm^2). The lower R_{ct} values for the NGnP4,6 CEs than those of the Pt counterpart suggest higher electrocatalytic activities for the reduction of $Co(bpy)_3^{3+}$ ions, which could enhance the current−voltage characteristics of DSSCs (in particular, FF and J_{sc}, but not the similar V_{oc}).

CONCLUSIONS

Nitrogen-doped graphene nanoplatelets (NGnP) were prepared by a simple and scalable two-step reaction sequence and evaluated as metal-free electrocatalysts for the reduction of $Co(bpy)_3^{3+}$ to replace the Pt CE in DSSCs. NGnP thin films on FTO deposited with an e-spray technique exhibited good electrocatalytic performances for the $Co(bpy)_3^{3+/2+}$ redox couple, in particular, lower charge transfer resistance (R_{ct}) at the interface of the NGnP-CE/electrolyte, and better electrochemical stability under prolonged cycling potential than those of the Pt counterpart. Notably, the extraordinarily better current−voltage characteristics of the DSSC-NGnP outperformed the DSSC-Pt for the $Co(bpy)_3^{3+/2+}$ redox couple (in particular, FF and J_{sc}). Thus, NGnP6 CE displayed a PCE of 9.05%, which was higher than that of the Pt CE by a factor of 1.07.

Our results suggest that the NGnP is a low-cost metal-free electrocatalyst to be used as a potential alternative material for the replacement of an expensive and scarce Pt CE in DSSCs with Co-complexed redox couple system.

EXPERIMENTAL SECTION

Preparation of NGnP and Pt Electrodes. Homogeneously dispersed 0.1 wt % NGnP powder in 2-propanol solution was obtained by ultrasonication for 30 min. The resultant solution was deposited directly onto FTO/glass (TEC-8, Pilkington) using an e-spray technique. First, the NGnP solution was loaded into a plastic syringe equipped with a 30-gauge stainless steel hypodermic needle. The needle was connected to a high voltage power supply (ESN-HV30). A voltage of ~10 kV was applied between a metal orifice and the conducting substrate at a distance of 10 cm. The feed rate was controlled by the syringe pump (KD Scientific Model 220) at a constant flow rate of 200 μL min^{-1}. The electric field overcomes the surface tension of the droplets, resulting in the minimization of numerous charged mists containing NGnP. The sample electrodes were sintered at 300 °C for 30 min under a nitrogen atmosphere prior to device fabrication. The optical spectra were measured by a Hewlett-Packard 8453 diode array spectrometer. A blank FTO sheet served as a reference electrode. In order to form a uniform thickness over a large area, the nozzle and substrate were placed on a motion control system using a microprocessor. The morphology of the NGnP electrodes was investigated using field emission scanning electron microscopy (FE-SEM, Hitachi S-4100). For comparison, a Pt CE was prepared by deposition of *ca.* 30 μL cm^{-2} of H_2PtCl_6 solution (2 mg of Pt in 1 mL of ethanol) and sintered at 400 °C for 15 min.

Fabrication of a Symmetrical Dummy Cell. A symmetrical sandwich dummy cell was fabricated from two identical NGnP- or Pt-FTO sheets, which were separated by 60-μm thick Surlyn (Solaronix, Switzerland) tape as a sealant and spacer leaving a 0.6 × 0.6 cm^2 active area. The sheet edges were coated by an ultrasonic soldering system (USS-9200, MBR Electronics) to improve electrical contacts. The cell was filled with an electrolyte solution of 0.22 M $Co(bpy)_3(BCN_4)_2$, 0.05 M $Co(bpy)_3(BCN_4)_3$, 0.1 M $LiClO_4$, and 0.8 M 4-*tert*-butylpyridine in acetonitrile through a hole in one FTO support, which was finally closed by a Surlyn seal. Co-complexes were synthesized following a previously published procedure.[45]

Electrochemical Analysis. All electrochemical measurements were carried out with a *VersaSTAT* 3 (Version 1.31), AMETEK connected to a potentiostat under dark conditions at room temperature. The EIS spectra were acquired in the frequency range from 10^6 to 0.1 Hz, at 0 V of open circuit voltage, and the AC modulation amplitude was 10 mV. EIS data analysis was processed using the Zplot/Zview software. The detailed fabrication and characterization of DSSCs were described in the Supporting Information.

Conflict of Interest: The authors declare no competing financial interest.

Acknowledgment. This work was supported by the Converging Research Center Program through the Ministry of Education, Science and Technology (2012K001287) and by the Human Resources Development Program (No. 20124010203190) of the Korea Institute of Energy Technology Evaluation and Planning (KETEP) Grant Funded by the Korea Government of Knowledge Economy.

Supporting Information Available: Additional experimental details and further analysis results. This material is available free of charge *via* the Internet at http://pubs.acs.org.

REFERENCES AND NOTES

1. O'Regan, B.; Grätzel, M. A Low-Cost, High Efficiency Solar Cell Based on Dye-Sensitized Colloidal TiO_2 Films. *Nature* **1991**, *353*, 737–740.
2. Grätzel, M. Photoelectrochemical Cells. *Nature* **2001**, *414*, 338–344.
3. Baek, N. S.; Yum, J.-H.; Zhang, X.; Kim, H. K.; Nazeeruddin, M. K.; Grätzel, M. Functionalized Alkyne Bridged Dendron Based Chromophores for Dye-Sensitized Solar Cell Applications. *Energy Environ. Sci.* **2009**, *2*, 1082–1087.
4. Murakami, T. N.; Ito, S.; Wang, Q.; Nazeeruddin, M. K.; Bessho, T.; Cesar, I.; Liska, P.; Humphry-Baker, R.; Comte, P.; Pechy, P.; et al. Highly Efficient Dye-Sensitized Solar Cells Based on Carbon Black Counter Electrodes. *J. Electrochem. Soc.* **2006**, *53*, A2255–A2261.
5. Jia, R.; Chen, J.; Zhao, J.; Zheng, J.; Song, C.; Li, L.; Zhu, Z. Synthesis of Highly Nitrogen-Doped Hollow Carbon Nanoparticles and Their Excellent Electrocatalytic Properties in Dye-Sensitized Solar Cells. *J. Mater. Chem.* **2010**, *20*, 10829–10834.
6. Yang, Z.; Chen, T.; He, R.; Guan, G.; Li, H.; Qiu, L.; Peng, H. Aligned Carbon Nanotube Sheets for the Electrodes of Organic Solar Cells. *Adv. Mater.* **2011**, *23*, 5436–5439.
7. Han, H.; Kim, H.; Kim, D. Y.; Jo, S. M.; Jang, S. Y. Water-Soluble Polyelectrolyte-Grafted Multiwalled Carbon Nanotube Thin Films for Efficient Counter Electrode of Dye-Sensitized Solar Cells. *ACS Nano* **2010**, *4*, 3503–3509.
8. Hong, W.; Xu, Y.; Lu, G.; Li, C.; Shi, G. Transparent Graphene/PEDOT-PSS Composite Films as Counter Electrodes of Dye-Sensitized Solar Cells. *Electrochem. Commun.* **2008**, *10*, 1555–1558.
9. Choi, H.; Kim, H.; Hwang, S.; Han, Y.; Jeon, M. Graphene Counter Electrodes for Dye-Sensitized Solar Cells Prepared by Electrophoretic Deposition. *J. Mater. Chem.* **2011**, *21*, 7548–7551.
10. Xu, Y.; Bai, H.; Lu, G.; Li, C.; Shi, G. Flexible Graphene Films *via* the Filtration of Water-Soluble Noncovalent Functionalized Graphene Sheets. *J. Am. Chem. Soc.* **2008**, *130*, 5856–5857.
11. Kavan, L.; Yum, J. H.; Grätzel, M. Optically Transparent Cathode for Dye-Sensitized Solar Cells Based on Graphene Nanoplatelets. *ACS Nano* **2011**, *5*, 165–172.
12. Jang, S.-Y.; Kim, Y.-G.; Kim, D. Y.; Kim, H.-G.; Jo, S. M. Electrodynamically Sprayed Thin Films of Aqueous Dispersible Graphene Nanosheets: Highly Efficient Cathodes for Dye-Sensitized Solar Cells. *ACS Appl. Mater. Interfaces* **2012**, *4*, 3500–3507.
13. Yang, S. B.; Feng, X. L.; Wang, X. C.; Mullin, M. Graphene-Based Carbon Nitride Nanosheets as Efficient Metal-Free Electrocatalysts for Oxygen Reduction Reactions. *Angew. Chem., Int. Ed.* **2011**, *50*, 5339–5343.
14. Gong, K.; Du, F.; Xia, Z.; Durstock, M.; Dai, L. Nitrogen-Doped Carbon Nanotube Arrays with High Electrocatalytic Activity for Oxygen Reduction. *Science* **2009**, *323*, 760–764.
15. Shao, Y.; Zhang, S.; Engelhard, M. H.; Li, G.; Shao, G.; Wang, Y.; Liu, J.; Aksay, I. A; Lin, Y. Nitrogen-Doped Graphene and Its Electrochemical Applications. *J. Mater. Chem.* **2010**, *20*, 7491–7496.
16. Xue, Y.; Liu, J.; Chen, H.; Wang, R.; Li, D.; Dai, L. Nitrogen-Doped Graphene Forms as Metal-Free Counter Electrodes in High-Performance Dye-Sensitized Solar Cells. *Angew. Chem., Int. Ed.* **2012**, *51*, 12124–12127.
17. Long, Y.; Zhang, C. C.; Wang, X. X.; Gao, J. P.; Wang, W.; Liu, Y. Oxidation of SO_2 to SO_3 Catalyzed by Graphene Oxide Foams. *J. Mater. Chem.* **2011**, *21*, 3934–13941.
18. Wan, L.; Wang, S.; Wang, X.; Dong, B.; Xu, Z.; Zhang, X.; Bing, Y.; Peng, S.; Wang, J.; Xu, C. Room-Temperature Fabrication of Graphene Films on Variable Substrates and Its Use as a Counter Electrodes for Dye-Sensitized Solar Cells. *Solid State Sci.* **2011**, *13*, 468–475.
19. Kavan, L.; Yum, J. H.; Grätzel, M. Graphene Nanoplatelets Outperforming Platinum as the Electrocatalyst in Co-Bipyridine-Mediated Dye-Sensitized Solar Cells. *Nano Lett.* **2011**, *11*, 5501–5506.

20. Su, D. S.; Zhang, J.; Frank, B.; Thomas, A.; Wang, X.; Paraknowitsch, J.; Schlogl, R. Metal-Free Heterogeneous Catalysis for Sustainable Chemistry. *ChemSusChem* **2010**, *3*, 169–180.
21. Yu, D. S.; Nagelli, E.; Du, F.; Dai, L. Metal-Free Carbon Nanomaterials Become More Active than Metal Catalysts and Last Longer. *J. Phys. Chem. Lett.* **2010**, *1*, 2165–2173.
22. Panchakarla, L. S.; Subrahmanyam, K. S.; Sala, S. K.; Govindayaj, A.; Krishnamurthy, H. R.; Waghmare, U. V.; Rao, C. N. R. Synthesis, Structure, and Properties of Boron- and Nitrogen-Doped Graphene. *Adv. Mater.* **2009**, *21*, 4726–4730.
23. Kurak, K. A.; Anderson, A. B. Nitrogen-Treated Graphite and Oxygen Electroreduction on Pyridinic Edge Sites. *J. Phys. Chem. C* **2009**, *113*, 6730–6734.
24. Roy-Mayhew, J. D.; Bozym, D. J.; Punckt, C.; Aksay, I. A. Functionalized Graphene as a Catalytic Counter Electrode in Dye-Sensitized Solar Cells. *ACS Nano* **2010**, *4*, 6203–6211.
25. Zhang, D. W.; Li, X. D.; Li, H. B.; Chen, S.; Sun, Z.; Yin, X. J.; Huang, S. M. Graphene-Based Counter Electrode for Dye-Sensitized Solar Cells. *Carbon* **2011**, *49*, 5382–5388.
26. Mattevi, C.; Eda, G.; Agnoli, S.; Miller, S.; Mkhoyan, K. A.; Celik, O.; Mostrogiovanni, D.; Granozzi, G.; Garfunkel, E.; Chhowalla, M. Evolution of Electrical, Chemical, and Structural Properties of Transparent and Conducting Chemically Derived Graphene Thin Films. *Adv. Funct. Mater.* **2009**, *19*, 2577–2583.
27. Yella, A.; Lee, H. W.; Tsao, H. N.; Yi, C.; Chandiran, A. K.; Nazeeruddin, M. K.; Diau, E. W. G .; Yeh, C. Y.; Zakeeruddin, S. M.; Grätzel, M. Porphyrin-Sensitized Solar Cells with Cobalt (II/III)-Based Redox Electrolyte Exceed 12% Efficiency. *Science* **2011**, *334*, 629–634.
28. Lim, K.; Kim, C.; Song, J.; Yu, T.; Lim, W.; Song, K.; Wang, P.; Zu, N.; Ko, J. Enhancing the Performance of Organic Dye-Sensitized Solar Cells *via* a Slight Structure Modification. *J. Phys. Chem. C* **2011**, *115*, 22640–22646.
29. Feldt, S. M.; Gibson, E. A.; Gabrielsson, E.; Sun, L.; Boschloo, G.; Hagfeldt, A. Design of Organic Dyes and Co Polypyridine Redox Mediators. *J. Am. Chem. Soc.* **2010**, *132*, 16714–16724.
30. Choi, E.-K.; Jeon, I.-Y.; Bae, S. Y.; Lee, H.-J.; Shin, H. S.; Dai, L.; Baek, J.-B. High-Yield Exfoliation of Three-Dimensional Graphite into Two-Dimensional Graphene-Like Sheets. *Chem. Commun.* **2010**, *46*, 6320–6322.
31. Jeon, I.-Y.; Yu, D.; Bae, S.-Y.; Choi, H.-J.; Chang, D. W.; Dai, L.; Baek, J.-B. Formation of Large-Area Nitrogen-Doped Graphene Film Prepared from Simple Solution Casting of Edge-Selectively Functionalized Graphite and Its Electrocatalytic Activity. *Chem. Mater.* **2011**, *23*, 3987–3992.
32. Park, S.; Ruoff, R. S. Chemical Methods for the Production of Graphenes. *Nat. Nanotechnol.* **2009**, *4*, 217–224.
33. Yu, Y.; Chen, C. H.; Shi, Y. A Tin-Based Amorphous Oxide Composite with a Porous, Spherical, Multideck-Cage Morphology as a Highly Reversible Anode Material for Lithium-Ion Batteries. *Adv. Mater.* **2007**, *19*, 993–997.
34. Chen, C. H.; Kelder, E. M.; VanderPut, P. J. J. M.; Schoonman, J. Morphology Control of Thin $LiCoO_2$ Films Fabricated Using the Electrostatic Spray Deposition (ESD) Technique. *J. Mater. Chem.* **1996**, *6*, 765–771.
35. Zhang, Y. Z.; Wu, L. H.; Xie, E. Q.; Duan, H. G.; Han, W. H.; Zhao, J. G. A Simple Method to Prepare Uniform-Size Nanoparticle TiO_2 Electrodes for Dye-Sensitized Solar Cells. *J. Power Sources* **2009**, *189*, 1256–1263.
36. Kim, J. H.; Nam, K. W.; Ma, S. B.; Kim, K. B. Fabrication and Electrochemical Properties of Carbon Nanotube Film Electrodes. *Carbon* **2006**, *44*, 1963–1968.
37. Hauch, A.; Georg, A. Diffusion in the Electrolyte and Charge-Transfer Reaction at the Platinum Electrode in Dye-Sensitized Solar Cells. *Electrochim. Acta* **2001**, *46*, 3457–3466.
38. Papageorgiou, N.; Maier, W. F.; Grätzel, M. An Iodine/Triiodide Reduction Electrocatalyst for Aqueous and Organic Media. *J. Electrochem. Soc.* **1997**, *144*, 876–884.
39. Fang, X.; Ma, T.; Guan, G.; Akiyama, M.; Kida, T.; Abe, E. Effect of the Thickness of the Pt Film Coated on a Counter Electrode on the Performance of a Dye-Sensitized Solar Cell. *J. Electroanal. Chem.* **2004**, *570*, 257–263.
40. Hagfeldt, A.; Boschloo, G.; Sun, L.; Kloo, L.; Pettersson, H. Dye-Sensitized Solar Cells. *Chem. Rev.* **2010**, *110*, 6595–6663.
41. Liberatore, M.; Petrocco, A.; Caprioli, F.; La Mesa, C.; Decker, F.; Bignozzi, C. A. Mass Transport and Charge Transfer Rates for Co(III)/Co(II) Redox Couple in a Thin-Layer Cell. *Electrochim. Acta* **2010**, *55*, 4025–4029.
42. Song, B. J.; Song, H. M.; Choi, I. K.; Kim, S. K.; Seo, K. D.; Kang, M. S.; Lee, M. J.; Cho, D. W.; Ju, M. J.; Kim, H. K. A Desirable Hole-Conducting Coadsorbent for Highly Efficient Dye-Sensitized Solar Cells through an Organic Redox Cascade Strategy. *Chem. Eur. J.* **2011**, *17*, 11115–11121.
43. Kang, M. S.; Kang, S. H.; Kim, S. K.; Choi, I. T.; Ryu, J. H.; Ju, M. J.; Cho, D.; Lee, J. Y.; Kim, H. K. Novel D$-\pi-$A Structured Zn(II)-Porphyrin Dyes Containing a Bis(3,3-dimethylfluorenyl)Amine Moiety for Dye-Sensitized Solar Cells. *Chem. Commun.* **2012**, *48*, 9349–9352.
44. Kang, S. H.; Choi, I. K.; Kang, M. S.; Eom, Y. K.; Ju, M. J.; Hong, J. Y.; Kang, H. S.; Kim, H. K. Novel D$-\pi-$A Structured Porphyrin Dyes with Diphenylamine Derived Electron-Donating Substituents for Highly Efficient Dye-Sensitized Solar Cells. *J. Mater. Chem. A* **2013**, *1*, 3977–3982.
45. Tsao, H. N.; Yi, C.; Moehl, T.; Yum, J. H.; Zakeeruddin, S. M.; Nazeeruddin, M. K.; Grätzel, M. Cyclopentadithiophene Bridged Donor-Acceptor Dyes Achieve High Power Conversion Efficiencies in Dye-Sensitized Solar Cells Based on Tris-Cobalt-Bipyridine Redox Couple. *ChemSusChem* **2011**, *4*, 591–594.